Experimental Investigations of Dam Break Flows down an Inclined Channel

D. Marra[1], T. Earl[2] and C. Ancey[1]
[1]Environmental Hydraulics Laboratory (LHE)
École Polytechnique Fédérale de Lausanne (EPFL)
CH-1015 Lausanne
SWITZERLAND
[2]School of Civil Engineering (JO5)
The University of Sydney
Sydney, NSW 2006
AUSTRALIA
E-mail: thomas.earl@sydney.edu.au

Abstract: *Dam break floods on steep slopes occur in diverse settings and can encompass natural events such as mudflows and avalanches as well as the failure of manmade dams. Laboratory experiments were undertaken to investigate the dam break flows of pure water down a variably sloping, rectangular fixed bed channel. A high-speed digital camera was used to track the flow. The images were processed to compute the front wave position and velocity, the maximum water height, the passing wave depth and the wave profile. The effects of varying the controlled parameters (i.e., the bed roughness and its inclination angle, the volume of water in the reservoir) were explored.*

Keywords: *dam-break flows, steep slopes, front velocity, image processing, high speed camera.*

1. INTRODUCTION

Dam break waves are extreme hydrologic events that occur in diverse settings. They may result due to the collapse of either natural or man-made dams and they have been responsible for huge economic and human losses. In the past years such overflow phenomena have been studied by many authors.

The analytical aspect, based on the shallow water equations, is important to test the robustness of numerical models. In this context, the first work was developed by Ritter (1892), who analysed the case of an infinite volume of water suddenly released on a frictionless horizontal plane. The exact solution of a finite volume of water on a frictionless horizontal bed was obtained by Hogg (2006). The more realistic investigation of the rough-bed case was analysed by a number of authors including Dressler (1952), Whitham (1955) and Hogg & Pritchard (2004), but only asymptotic solutions have been obtained to date. For the sloping bed case, exact solutions regarding ideal fluid were obtained for an infinite volume by Karelsky *et al* (2000) and Peregrine & Williams (2001), for a finite volume by Ancey *et al*. (2008) and from a theoretical point of view by Chanson (2009). In addition, the influence of the frictional effects due to the bed stress on the flow of a finite volume of fluid suddenly released on a steep slope was recently investigated by Bohorquez (2010).

From the experimental perspectives, there are works that dealt with horizontal beds with the configuration of pure water with fixed bed (Lauber & Hager, 1998a); water mixed with sediment over a fixed bed (Boillat *et al,* 2008), and water mixed with sediment over a movable bed (Capart & Young, 1998; Chanson *et al,* 2000; Spinewine & Zech, (2007); Leal *et al* 2006; Leal *et al,* 2009). Surprisingly, the case of inclined bed, despite its importance, is relatively poorly investigated from an experimental aspect; the only important studies address the case of pure water, an example of which performed by Lauber & Hager, (1998b). Moving towards a larger scale, there was a dam break investigation performed by USGS (Iverson *et al,* 1992; Denlinger & O'Connel, 2008).

The present experimental work places itself in the context described above. The investigation covered a range of pure water-driven dam break experiments on an inclined channel where the influence of the volume of water, V, bed inclination, α, and bed roughness, D, on the main characteristics of the wave were investigated. The analysis was performed by means of processing digital images of the experiment recorded by a high speed camera.

2. EXPERIMENTAL SET UP

The experiments were carried out in the Environmental Hydraulics Laboratory (LHE) at the École Polytechnique Fédérale de Lausanne (EPFL). A 3 metre long, 10 centimetre wide channel made of two vertical glass walls and an aluminium bottom was built for the experiments (Figure 1). An upstream reservoir was connected to the channel by a gate perpendicular to the bottom that could be opened suddenly by two pneumatic jacks simulating a rapid dam break (it took the gate 0.25s to open completely). The channel inclination could be varied between 0 and 45° with a precision of 0.1°, the reservoir being fully fixed to the channel with common bed angle. In order to test for the effects of varying the bed roughness, three different types of fixed channel beds were considered: an aluminium plate smooth bed and two different rough beds realised by glass beads fixed to the aluminium plate itself, with nominal diameters, D of 0.75-1mm (with Manning coefficient, n, of 0.0133 $m^{-1/3}s$) and D of 2mm (n of 0.0153 $m^{-1/3}s$) (Jäggi, 1984).

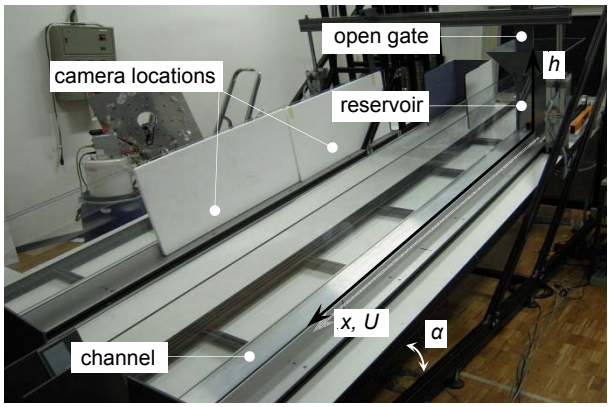

Figure 1: Picture of the experimental set-up.

Table 1: Values of the investigated parameters.

Volume of water [L]	3, 4, 5, 6, 7, 8
Channel inclination [°]	1.5, 3, 6, 9, 12, 16, 20, 24
Bed type	Smooth Bed, D = 0.75-1mm, D = 2mm

2.1. Images recording and processing

The investigation covered a range of approximately 340 separate experiments in order that all combinations of the parameters reported in Table 1 were investigated. Each experiment was recorded by a high speed camera (BASLER A504k with CMOS sensor) that took between 500-800 shots per second for a total of 1000-4000 shots per experiment (depending on the inclination of the bed). It was necessary to capture the first and second metre of the channel in two separate experiments and to illuminate the channel with 4000W to achieve the required optical resolution.
Figure 2 shows an example of the recorded images, for α = 24°, V = 6 L, D = 0.75-1 mm, for t = 0.25s and t = 0.8 s, being t the time after the dam failure (i.e. the first instance of the gate opening).

Figure 2: Recorded images for α = 24°, V = 6 L, D = 0.75 - 1mm; a) first meter recording, t = 0.25s; b) second meter recording, t = 0.8s.

The images were processed using the commercial software *MatLab*. The scripts exploited the contrast between the water (dyed blue) and the channel walls, which enabled the automatic tracking of the front position and profile of each wave. The images were calibrated from 10 mm spaced grids placed in the channel before the experiments were undertaken; each pixel was assigned a length-per-pixel value. It was then possible to 'stitch' the first to the corresponding second metre of each experiment from the two camera perspectives; the continuity of this process gave confidence of experimental repeatability.

3. EXPERIMENTAL RESULTS

Considering the downstream distance to the dam section measured from the reservoir gate, x, the water depth perpendicular to the channel bed, h, the initial water depth behind the reservoir gate, H_0, the maximum water depth in a fixed section (using the back profile of the wave), H_{MAX}, and the front velocity, U, by means of dimensionless coordinates we have:

$$x' = x / H_0 \quad (1)$$

$$t' = t / \sqrt{H_0 / (g \cdot \cos\alpha)} \quad (2)$$

$$U' = U / \sqrt{H_0 \cdot g \cdot \cos\alpha} \quad (3)$$

$$H'_{MAX} = H_{MAX} / H_0 \quad (4)$$

where the prime indicates a dimensionless variable and g is the gravity acceleration. The following analyses were conducted: dimensionless front wave position ($t' = f(x')$); dimensionless front wave velocity as a function of dimensionless downstream distance ($U' = f(x')$); water depth profile for a fixed time as a function of downstream distance ($h(t) = f(x)$); water depth profile measured from a fixed point as a function of time ($h(x) = f(t)$); dimensionless maximum water depth as a function of the dimensionless downstream distance ($H'_{MAX} = f(x')$).

3.1. Front Position

Figure 3 shows ($t' = f(x')$) for the three bed types considered in the investigation and for four of the eight analysed bed inclinations (α = 3°, 9°, 16°, 24°): this expression, for the same α and D, gave a unique curve independently from V. It can be observed that an increase of the bed roughness results in a decrease of the front position velocity. Moreover it can be seen that the effect of the roughness decreases as the bed inclination increases: this is a result of the gravitational effects becoming more predominant along an increasing downstream length compared to the viscous effects.

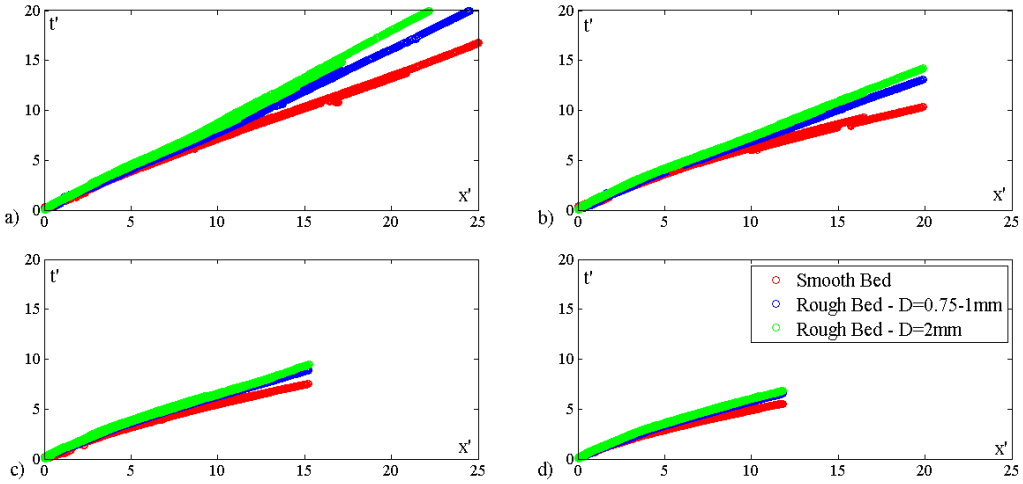

Figure 3: Dimensionless front position as a function of dimensionless time; a) α = 3°, b) α = 9°, c) α = 16°, d) α = 24°.

3.1.1. Data Fitting

The experimental results have been fitted with the power law:

$$t' = a \cdot x'^{b} \tag{5}$$

With robustness confirmed by an R^2 value no less than 99% for all experiments. Figure 4 shows the variation of coefficients *a* and *b* as a function of α and their empirical approximation by (6) and (7).

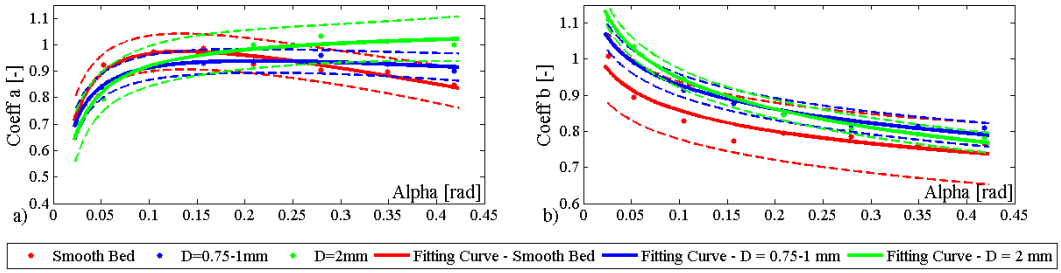

Figure 4: a) Coefficient *a as a* function of α for the three bed type and its fitting curves (6); b) coefficient *b* as a function of α for the three bed types and its fitting curves (7); dotted line: 95% confidence bounds.

$$a(\alpha) = \frac{g_1 \cdot \alpha^2 + g_2 \cdot \alpha}{\alpha + g_3} \tag{6}$$

$$b(\alpha) = e_1 \cdot \log(\alpha) + e_2 \tag{7}$$

The values of the coefficient of Eq. (6) and Eq. (7) and their R^2values are reported in Table 2.
It should be noted that Eq. (5) in a log-log plane represents a straight line where the coefficient *b* is its slope. From Figure 4a it can be noted that, increasing α, the experimental coefficient *a* tends to reach an asymptotic value of approximately 0.9; from Figure 4b we can observe that *b* has values around 1 for small inclinations (1.5°, 3°) and it decreases toward an anticipated asymptotic value of approximately 0.7 for steeper inclinations (20°, 24°). Furthermore we can observe that *b* is approximately 10% smaller for the smooth bed case with respect to the two analysed rough beds (where *b* has more or less the same magnitude).

Table 2: Coefficients g_1, g_2, g_3 and value of R^2 for Eq. (6) and e_1, e_2 and R^2 value for Eq. (7).

Bed Type	Coefficients of Eq. (6)				Coefficients of Eq.(7)		
	g_1	g_2	g_3	R^2	e_1	e_2	R^2
Smooth Bed	-0.730	1.172	0.0139	0.94	-0.083	0.666	0.89
D = 0.75-1 mm	-0.229	1.035	0.0109	0.97	-0.096	0.707	0.99
D = 2 mm	0.0300	1.043	0.0139	0.97	-0.124	0.661	0.99

3.2. Wave Front Velocity

The wave front velocity was determined from the corresponding front position using $U = (x_{t+n} - x_t) / n \cdot \Delta t$ where Δt is the time between camera shots and $n \in \mathbb{N} > 0$ was used to facilitate an average velocity which was required due to the volatility of the expression as a result of the high acquisition frequency. The dimensionless front wave velocity, U', (determined from U with n = 25) as a function of the dimensionless downstream distance to the dam section, x', ($U' = f(x')$) is reported in Figure 5.
It can be noted that the velocity profile is less smooth for a corresponding increase of the bed roughness and the bed inclination due to the presence of growing instabilities such as roll waves (Bohorquez, 2010). Thanks to an equilibrium being reached between the viscous shear effects and the gravitational forces, U', for the rough beds, was observed to reach a mean asymptotic value for an α of less than and equal to 16° while for the smooth bed with α greater than 3° no such asymptote was observed: this is due by the fact that, for these cases, the equilibrium between gravitational and frictional forces would be reached later, if the channel was longer.

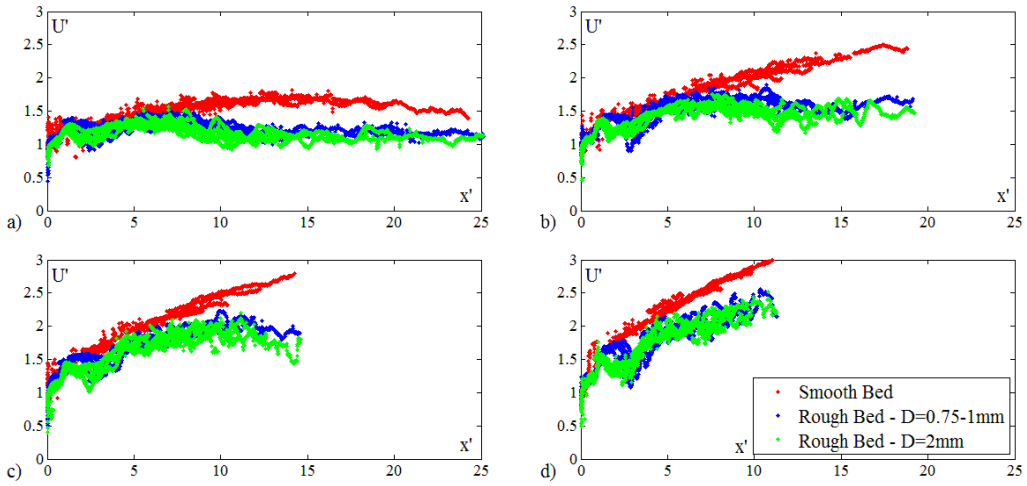

Figure 5: Dimensionless front velocity; a) α = 3°, b) α = 9°, c) α = 16°, d) α = 24°.

3.3. Wave Depth Profile

The water depth profiles of the wave ($h(t) = f(x)$) were recovered and one example for α = 24° , for the three analysed bed types, for V=3 and 6 L, at different time steps is shown in Figures 6. The most interesting observation to note from the wave depth profiles is the secondary wave that has reflected off the back wall of the reservoir. As one would expect, the roughness of the bed tends to form a rounded and more pronounced toe on the front position, where the smooth bed case is flatter. For a consistent α, an increase in volume generates a profile that is deeper and faster. While the channel inclination increases, the profile is less and less smooth due to the aforementioned instabilities.

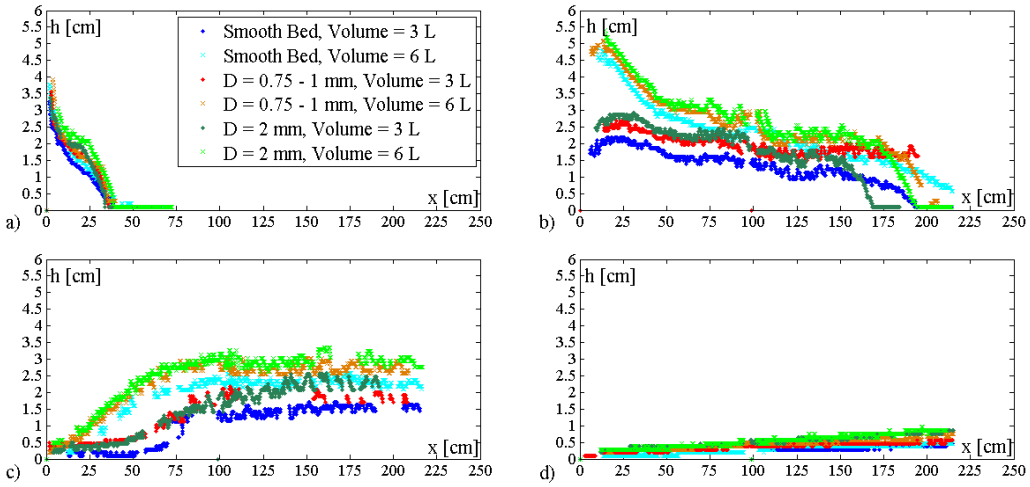

Figure 6: Water depth along the channel for α = 24°, for the three bed roughness cases and for water volumes equal to 6 and 3 litres; a) t = 0.25s, b) t = 0.8s, c) t = 1.2s, d) t = 2s.

3.4. Passing Wave Depth

At a number of predefined fixed positions, the passing wave depth was measured ($h(x) = f(t)$), and the 6 litre experiments over a range of inclinations are presented in Figure 7. One can draw several important conclusions from these observing that as α decreases: the passing wave depth is less and tends to form a smoother peak with a longer and deeper tail; the peak depth occurs later after the dam break, and; the entire water volume tends to evacuate the channel less rapidly. When comparing the same inclinations with different bed roughness, no such observations can be made: in particular it can be noted that, for the same α and the same x, the peak occurs at the same time t.

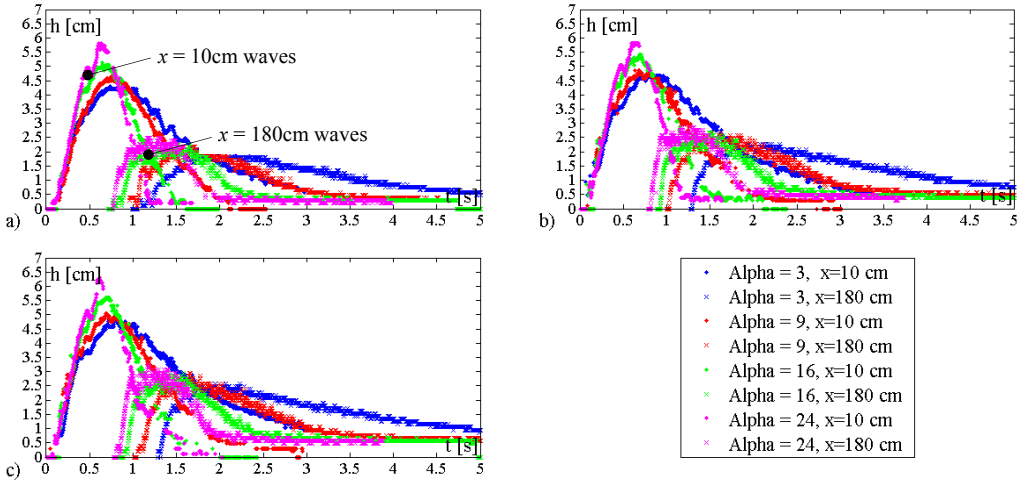

Figure 7: Passing wave depth, measured at x = 10 cm and x = 180 cm, for four analysed angles and for a water volume of 6 litres; a) Smooth bed, b) D = 0.75-1 mm, c) D = 2 mm.

3.5. Maximum Water Height

The dimensionless maximum water height that occurred at x' (H'_{MAX}= $f(x')$) is plotted in Figure 8. It can be seen that for an increase in α, the maximum water height curves more steeply toward an anticipated asymptote of an H'_{MAX} of approximately 0.1 (a value common of the inclination range reported in this paper). Moreover, the variability of H'_{MAX}= $f(x')$ is less and less intense while increasing the channel inclination.

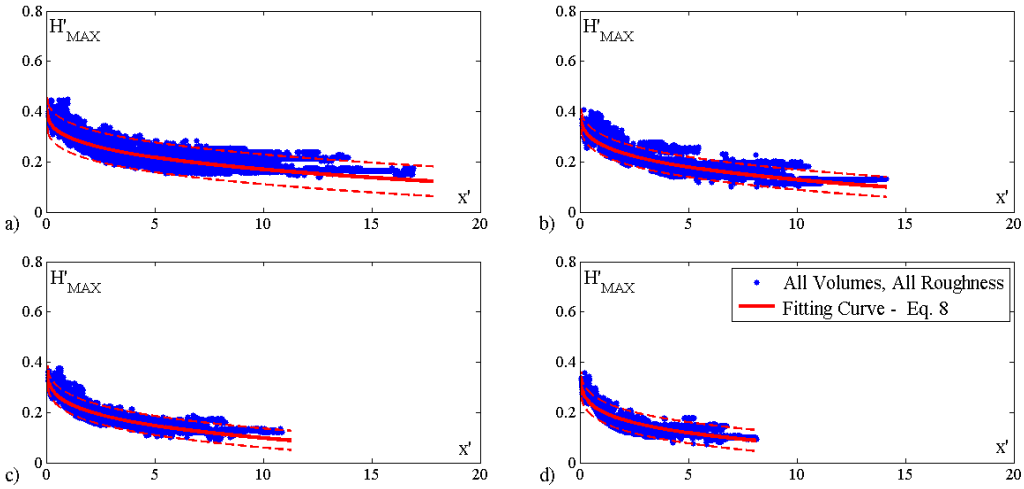

Figure 8: Dimensionless H_{MAX} and fitting curves Eq. (8) for all of the roughness cases and water volumes (dotted line: 95% confidence bounds); a) α = 3°, b) α = 9°, c) α = 16°, d) α = 24°.

3.5.1. Data Fitting

The experimental results are fitted the expression:

$$H'_{MAX} = \frac{r \cdot x' + \frac{4}{9} \cdot s}{x' + s} \tag{8}$$

As for Lauber & Hager (1998b), a constraint of 4/9 was applied to H'_{MAX} in Eq. (8) for x' = 0, according to the analytical solution of Ritter (1892). The coefficients r and s as a function of α are fitted with the laws:

$$r(\alpha) = p_1 \cdot \alpha + p_2 \tag{9}$$

$$s(\alpha) = q_1 \cdot \log(\alpha) + q_2 \tag{10}$$

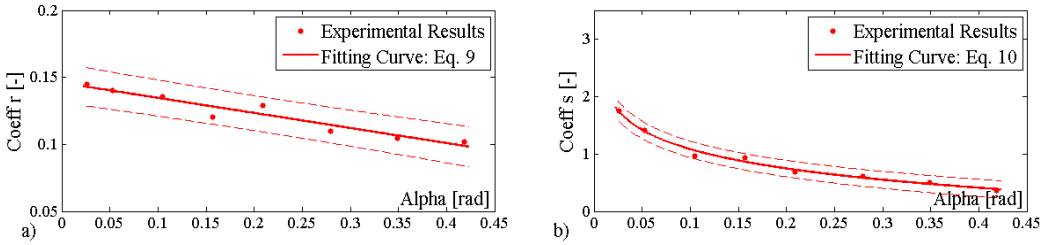

Figure 9: a) Coefficient *r* as a function of α for the three bed types, all the water volumes and their fitting curves Eq. (9); b) Coefficient *s* in function of α for the three bed type and all the water volumes and its fitting curves Eq. (10); dotted line: 95% confidence bounds.

From Figure 9 it is shown that the coefficients of the trend line of Eq. (9) and (10) have good regression. The values of the coefficients and of the regression are displayed in Table 3.

Table 3: Coefficients p_1, p_2, and value of R^2 for the Eq. (9) and q_1, q_2 and value of R^2 for Eq. (10).

Coefficients of Eq. (9)			Coefficients of Eq. (10)		
p_1	p_2	R^2	q_1	q_2	R^2
-0.112	0.146	0.92	-0.484	-0.035	0.99

4. CONCLUSION

The salient characteristics of a dam break wave down a variably sloping, rectangular fixed bed channel have been reported while investigating the effects of bed roughness, inclination, and water volume. The experiments have been recorded by a high-speed digital camera running between 500-800 Hz. The processing of the images allowed the determination of the main characteristics of the generated water waves. The continuity of results observed over the 1 m transition where camera locations changed indicates good experimental repeatability. It was found that various dimensionless variables were applicable to some of the results ($t' = f(x')$, ($U' = f(x')$, $H'_{MAX} = f(x')$) that avoided to take into account the explicit influence of the water volume in the reservoir. In particular it has been found that the bed roughness produces some instabilities in the wave front velocity and in the water depth profile. Moreover, as the bed roughness increases, for a fixed α, the front becomes slower and its form is more rounded. The regression analysis of the raw data and trends of the data fitting coefficients could be particularly useful for scaling and extrapolating the flows to full scale. Further investigations that are currently underway include the comparison with numerical solutions, the influence of sediment presence in the reservoir and the moveable bed configuration.

5. ACKNOWLEDGEMENTS

This investigation was developed in accordance to the frame of the APUNCH research project (http://www.cces.ethz.ch/projects/hazri/apunch) funded by the Competence Center Environment and Sustainability (CCES).

6. REFERENCES

Ancey C., Iverson R.M., Rentschler M. and Denlinger R.P. (2008), *An exact solution for ideal dam-break floods on steep slopes*, Water Resour. Res., 44, W01430.

Bohorquez P. (2010), *Competition between kinematic and dynamic waves in floods on steep slopes*, J. Fluid Mech., 645, 375-409.

Boillat J.L., Ribeiro J., Duarte R. and Darbre G. (2008), *Dam break in case of silted-up reservoirs*, in Altinakar, M.S., and al. (Eds), *Proceed. of River Flow 2008*, Çesme, 6-8 September, 2008, pp. 689-695.

Capart H., Young D.L. (1998), *Formation of a jump by the dam-break wave over a granular bed*, J. Fluid Mech., 372, 165-187.

Chanson H. (2009), *Application of the method of characteristics to the dam break wave problem*, J. Hydraul. Res., 47 (1), 41-49.

Chanson H., Aoki S. and Maruyama M. (2000), *Experimental investigations of wave run up downstream of nappe impact. Applications to flood wave resulting from dam overtopping and tsunami wave run up*, Coastal/Ocean Engineering Report No. COE00-2, Dept. of Architecture and Civil Eng., Toyohashi University of Technology, Japan, 38.

Denlinger R.P. and O'Connell R.H. (2008), *Computing Non-hydrostatic Shallow-Water Flow over Steep Terrain*, J. Hydraul. Eng., 134 (11), 1590-1602.

Dressler, R.F. (1952), *Hydraulic resistance effect upon the dam break functions*. J. Res. Natl. Bureau of Standards, 49(3), 217–225.

Hogg A. J. (2006), *Lock-release gravity currents and dam-break flows*, J. Fluid Mech., 569, 61-87.

Hogg A.J., and Pritchard D. (2004), *The effects of hydraulic resistance on dam-break and other shallow inertial flows*, J. Fluid Mech., 501, 179-212.

Iverson R.M., Costa J.E. and LaHusen R.G. (1992), *Debris-flow flume at H.J. Andrews Experimental Forest, Oregon*, U.S. Geological Survey Open File Rep. N. 92-483.

Jäggi M. (1984), *Abflußberechnung in kiesführenden Flüssen,* Wasserwirtschaft, Friedrich Vieweg, Wiesbaden, Germany, 74(5), 263-267 (in German).

Karelsky K.V., Papkov V.V., Petrosyan A.S. and Tsygankov D.V. (2000), *The initial discontinuity decay problem for shallow water equations on slopes*, Phys. Lett. A, 271, 349-357.

Lauber G. and Hager W.H. (1998), *Experiments to dambreak wave: Horizontal channel*, J. Hydraul. Res., 36 (3), 291-307.

Lauber G. and Hager W.H. (1998), *Experiments to dambreak wave: Sloping channel*, J. Hydraul. Res., 36 (5), 291-307.

Leal J.G.A.B., Ferreira R.M.L. and Cardoso A.H. (2009), *Maximum Level and Time to Peak of Dam-Break Waves on Mobile Horizontal Bed*, J. Hydraul. Eng., 135 (11), 995-999.

Leal J.G.A.B., Ferreira R.M.L. and Cardoso A.H. (2006), *Dam-Break Wave-Front Celerity*, J. Hydraul. Eng., 132 (1), 69-76.

Peregrine D.H. and Williams S.M. (2001), *Swash overtopping a truncated plane beach*, J. Fluid Mech., 440, 391-399.

Ritter A. (1892), *Die Fortpflanzung von Wasserwellen*, Zeitschrift Verein Deutscher Ingenieure, 36 (33), 947-954 (in German).

Spinewine B., Zech Y. (2007), *Small-scale laboratory dam-break waves on movable beds*, J. Hydraul. Res., 45 (Extra Issue), 73-86.

Whitham G.B. (1954), *The effects of hydraulic resistance in the dambreak problem*, Proc. R. Soc. London Ser. A, 227, 399-407.